Nonlinear excitation of polariton cavity modes in ZnO single nanocombs

M.G. Capeluto,[1,2,*] G. Grinblat,[1,3,4] M. Tirado,[5] D. Comedi,[3,4] and A.V. Bragas[1,2]

[1]*Laboratorio de Electrónica Cuántica, Depto. de Física, FCEyN, UBA, 1428 Buenos Aires, Argentina*
[2]*IFIBA-CONICET-UBA, 1428 Buenos Aires, Argentina*
[3]*Laboratorio de Física del Sólido, Depto. de Física, FACET, UNT, 4000 S.M. de Tucumán, Argentina*
[4]*CONICET, Argentina*
[5]*Laboratorio de Nanomateriales y de Propiedades Dieléctricas, Depto. de Física, FACET, UNT, 4000 S.M. de Tucumán, Argentina*
**maga@df.uba.ar*

Abstract: Tunable second harmonic (SH) polaritons have been efficiently generated in ZnO nanocombs, when the material is excited close to half of the band-gap. The nonlinear signal couples to the nanocavity modes, and, as a result, Fabry-Pérot resonances with high Q factors of about 500 are detected. Due to the low effective volume of the confined modes, matter-light interaction is very much enhanced. This effect lowers the velocity of the SH polariton in the material by 50 times, and increases the SH confinement inside the nanocavity due to this higher refractive index. We also show that the SH phase-matching condition is achieved through LO-phonon mediation. Finally, birrefringence of the crystal produces a strong SH intensity dependence on the input polarization, with a high polarization contrast, which could be used as a mechanism for light switching in the nanoscale.

OCIS codes: (190.5970) Semiconductor nonlinear optics including MQW; (160.4236) Nanomaterials; (140.3945) Microcavities.

References and links

1. J. C. Johnson, H. Yan, P. Yang, and R. J. Saykally, "Optical cavity effects in ZnO nanowire lasers and waveguides," J. Phys. Chem. B **107**(34), 8816–8828 (2003).
2. L. K. van Vugt, S. Rühle, P. Ravindran, H. C. Gerritsen, L. Kuipers, and D. Vanmaekelbergh, "Exciton polaritons confined in a ZnO nanowire cavity," Phys. Rev. Lett. **97**(14), 147401 (2006).
3. W. Li, M. Gao, X. Zhang, D. Liu, L.-M. Peng, and S. Xie, "Microphotoluminesce study of exciton polaritons guided in ZnO nanorods," Appl. Phys. Lett. **95**(17), 173109 (2009).
4. H. Y. Li, S. Rühle, R. Khedoe, A. F. Koenderink, and D. Vanmaekelbergh, "Polarization, Microscopic Origin, and Mode Structure of Luminescence and Lasing from Single ZnO Nanowires," Nano Lett. **9**(10), 3515–3520 (2009).
5. S. L. Chen, W. M. Chen, and I. A. Buyanova, "Slowdown of light due to exciton-polariton propagation in ZnO," Phys. Rev. B **83**(24), 245212 (2011).
6. C. Sturm, H. Hilmer, B. Rheinländer, R. Schmidt-Grund, and M. Grundmann, "Cavity-photon dispersion in one-dimensional confined microresonator with an optically anisotropic cavity material," Phys. Rev. B **83**(20), 205301 (2011).
7. A. Das, J. Heo, A. Bayraktaroglu, W. Guo, T. K. Ng, J. Phillips, B. S. Ooi, and P. Bhattacharya, "Room temperature strong coupling effects from single ZnO nanowire microcavity," Opt. Express **20**(11), 11830–11837 (2012).
8. F. Li, L. Orosz, O. Kamoun, S. Bouchoule, C. Brimont, P. Disseix, T. Guillet, X. Lafosse, M. Leroux, J. Leymarie, G. Malpuech, M. Mexis, M. Mihailovic, G. Patriarche, F. Réveret, D. Solnyshkov, and J. Zuniga-Perez, "Fabrication and characterization of a room-temperature ZnO polariton laser," Appl. Phys. Lett. **102**(19), 191118 (2013).
9. T. C. Lu, Y. Y. Lai, Y. P. Lan, S. W. Huang, J. R. Chen, Y. C. Wu, W. F. Hsieh, and H. Deng, "Room temperature polariton lasing vs. photon lasing in a ZnO-based hybrid microcavity," Opt. Express **20**(5), 5530–5537 (2012).
10. C. F. Klingshirn, *Semiconductor Optics* (Springer, 2005).
11. M. H. Huang, S. Mao, H. Feick, H. Yan, Y. Wu, H. Kind, E. Weber, R. Russo, and P. Yang, "Room-temperature ultraviolet nanowire nanolasers," Science **292**(5523), 1897–1899 (2001).
12. D. Vanmaekelbergh and L. K. van Vugt, "ZnO nanowire lasers," Nanoscale **3**(7), 2783–2800 (2011).

#197588 - $15.00 USD Received 12 Sep 2013; revised 25 Nov 2013; accepted 5 Jan 2014; published 28 Feb 2014

13. J. Dai, J. H. Zeng, S. Lan, X. Wan, and S. L. Tie, "Competition between second harmonic generation and two-photon-induced luminescence in single, double and multiple ZnO nanorods," Opt. Express **21**(8), 10025–10038 (2013).
14. J. C. Johnson, H. Yan, R. D. Schaller, P. B. Petersen, P. Yang, and R. J. Saykally, "Near-field imaging of nonlinear optical mixing in single zinc oxide nanowires," Nano Lett. **2**(4), 279–283 (2012).
15. S. K. Das, M. Bock, C. O'Neill, R. Grunwald, K. Lee, H. W. Lee, S. Lee, and F. Rotermund, "Efficient second harmonic generation in ZnO nanorod arrays with broadband ultrashort pulses," Appl. Phys. Lett. **93**(18), 181112 (2008).
16. S. L. Shi, S. J. Xu, Z. X. Xu, V. A. L. Roy, and C. M. Che, "Broadband second harmonic generation from ZnO nano-tetrapods," Chem. Phys. Lett. **506**(4-6), 226–229 (2011).
17. J. I. Jang, S. Park, N. L. Frazer, J. B. Ketterson, S. Lee, B. K. Roy, and J. Cho, "Strong P-band emission and third harmonic generation from ZnO nanorods," Solid State Commun. **152**(14), 1241–1243 (2012).
18. S. W. Chan, E. Barille, J. M. Nunzi, K. H. Tam, Y. H. Leung, W. K. Chan, and A. B. Djurišić, "Second harmonic generation in zinc oxide nanorods," Appl. Phys. B **84**(1–2), 351–355 (2006).
19. X. Lu, H. Zhou, G. J. Salamo, Z. R. Tian, and M. Xiao, "Generation of exciton-polaritons in ZnO microcrystallines using second-harmonic generation," New J. Phys. **14**(7), 073017 (2012).
20. G. Grinblat, M. G. Capeluto, M. Tirado, D. Comedi, and A. V. Bragas, "Two-photon photoluminescence from hierarchical ZnO nanostructures," ECS Trans. **45**(5), 67–72 (2012).
21. K. J. Vahala, "Optical microcavities," Nature **424**(6950), 839–846 (2003).
22. U. Ozgur, Ya. I. Alivov, C. Liu, A. Teke, M. A. Reshchikov, S. Dogan, V. Avrutin, S.-J. Cho, and H. Morkoc, "A comprehensive review of ZnO materials and devices," J. Appl. Phys. **98**(4), 041301 (2005).
23. A. B. Djurisić, W. M. Kwok, Y. H. Leung, D. L. Phillips, and W. K. Chan, "Stimulated emission in ZnO nanostructures: A time-resolved study," J. Phys. Chem. B **109**(41), 19228–19233 (2005).
24. A. B. Djurisić and Y. H. Leung, "Optical properties of ZnO nanostructures," Small **2**(8-9), 944–961 (2006).
25. M. H. Huang, S. Mao, H. Feick, H. Yan, Y. Wu, H. Kind, E. Weber, R. Russo, and P. Yang, "Room-temperature ultraviolet nanowire nanolasers," Science **292**(5523), 1897–1899 (2001).
26. G. Grinblat, M. G. Capeluto, M. Tirado, A. V. Bragas, and D. Comedi, "Hierarchical ZnO nanostructures: Growth mechanisms and surface correlated photoluminescence," Appl. Phys. Lett. **100**(23), 233116 (2012).
27. T. L. Phan, Y. Sun, and R. Vincent, "Structural characterization of CVD-grown ZnO nanocombs," J. Korean Phys. Soc. **59**(1), 60–64 (2011).
28. C. H. Zang, Y. C. Liu, D. X. Zhao, J. Y. Zhang, and D. Z. Shen, "The synthesis and optical properties of ZnO nanocombs," J. Nanosci. Nanotechnol. **10**(4), 2370–2374 (2010).
29. D. W. Hamby, D. A. Lucca, D. J. Klopfstein, and G. Cantwell, "Temperature dependent exciton photoluminescence of bulk ZnO," J. Appl. Phys. **93**(6), 3214–3217 (2003).
30. J. Lagois, "Depth-dependent eigenenergies and damping of excitonic polaritons near a semiconductor surface," Phys. Rev. B **23**(10), 5511–5520 (1981).
31. A. Takagi, A. Nakamura, A. Yoshikaie, S. Yoshioka, S. Adachi, S. F. Chichibu, and T. Sota, "Signatures of Γ1-Γ5 mixed-mode polaritons in polarized reflectance spectra of ZnO," J. Phys. Condens. Matter **24**(41), 415801 (2012).
32. S. W. Jung, W. I. Park, H. D. Cheong, G. C. Yi, H. M. Jang, S. Hong, and T. Joo, "Time-resolved and time-integrated photoluminescence in ZnO epilayers grown onAl_2O_3(0001) by metalorganic vapor phase epitaxy," Appl. Phys. Lett. **80**(11), 1924 (2002).
33. D. C. Dai, S. J. Xu, S. L. Shi, M. H. Xie, and C. M. Che, "Efficient multiphoton-absorption-induced luminescence in single-crystalline ZnO at room temperature," Opt. Lett. **30**(24), 3377–3379 (2005).
34. L. K. van Vugt, B. Piccione, C. H. Cho, P. Nukala, and R. Agarwal, "One-dimensional polaritons with size-tunable and enhanced coupling strengths in semiconductor nanowires," Proc. Natl. Acad. Sci. U.S.A. **108**(25), 10050–10055 (2011).
35. N. S. Han, H. S. Shim, S. Lee, S. M. Park, M. Y. Choi, and J. K. Song, "Light-matter interaction and polarization of single ZnO nanowire lasers," Phys. Chem. Chem. Phys. **14**(30), 10556–10563 (2012).
36. M. Gao, R. Cheng, W. Li, Y. Li, X. Zhang, and S. Xie, "Directly probing the anisotropic optical emission of individual ZnO nanorods," J. Phys. Chem. C **114**(25), 11081–11086 (2010).
37. U. Choppali and B. P. Gorman, "Effect of annealing on room temperature photoluminescence of polymeric precursor derived ZnO thin films on sapphire substrates," Opt. Mater. **31**(2), 143–148 (2008).
38. Maria Cristina Larciprete, and Mario Bertolotti, "Second harmonic generation and related studies on ZnO films" in *Handbook of zinc oxide and related materials, Part II*, Zhe Chuan Feng eds. (CRC Press., 2013), pp. 141–166.

1. Introduction

Optoelectronics circuitry at the micro-nanoscale requires the fabrication of devices with a high efficiency of light generation in a wide range of the spectrum. Linear optical properties of semiconductor microwires, nanowires and microcavities have been extensively studied in the last years, particularly in semiconductors with a large band-gap [1–7], which operate in the blue and UV. The interest in those materials such as ZnO, lies mainly in their large exciton oscillator strength and binding energy, which allows, for instance, the possibility to build room-temperature polariton lasers [8, 9] at the nanoscale. Optical and structural properties of ZnO have been studied since the first half of the last century but it was virtually

#197588 - $15.00 USD Received 12 Sep 2013; revised 25 Nov 2013; accepted 5 Jan 2014; published 28 Feb 2014

abandoned for a long time, among other reasons, due to the early difficulty to realize p-doping in this semiconductor [10]. However, a renewed interest in this material grew in the optical community in the last decade after the demonstration of laser emission from ZnO nanowires [11], followed by a great amount of work on the optical properties of nano-micro devices based on ZnO [12]. Nevertheless the majority of these studies on ZnO only acknowledge the linear properties of the optical response. However there are many relevant works on its non linear properties, some of them listed in Refs. [13–20]. Indeed, nonlinear emission devices can be an important part of the toolbox of components needed for nanophotonics and integrated circuits at the nanoscale. As an example, the efficient nonlinear optical emission such as second harmonic (SH) generation, may enable frequency conversion at the nanoscale as well as the development of ultrafast switching mechanisms due to the SH polarization selectivity.

Numerous designs of microcavities or microresonators have been proposed in recent years with the aim to confine, guide and amplify the light through optoelectronic devices [9, 21]. However, the epitaxial growth of these large band-gap materials is challenging, which makes the design of low-losses cavities quite difficult. In this context, optical cavities designed from nano-objects of ZnO have become relevant, because of the varied and numerous growing techniques which provide materials with high crystal quality, and, at the same time, cheap and fast production [22]. The evident weak point is that the mirrors of the cavity are just given by the change of the optical impedance or the refractive indices between ZnO and the surroundings, although ZnO has a high refractive index (about 2, far from resonances). Still, lasing has been demonstrated for a variety of different ZnO morphologies [23–25], while the lasing mechanism is not fully understood in all the cases.

In this work, we show efficient SH generation in birefringent ZnO nanocombs (NCs) exciting nearby excitonic resonances. The low effective volume cavity selects the mode with wavevector k_{SH}//c, and confines the SH light in the NCs teeth, so that the emission shows Fabry-Pérot (FP) modes with high quality factors on the order of 500. The high reflectivity on the end facets of the nanocavity is due to a huge ZnO refractive index increment produced by a strong light-nanocavity coupling. This interaction leads to a 50 times lowering of the SH polariton propagation velocity with respect to the propagation velocity calculated by using the refraction index far from resonances. We also show that by rotating the input polarization, the emission changes from a high-intensity to a low-intensity state, following the polarization rules of the birefringent material nonlinear response. In addition, we measured the contrast between these two intensity states and found that it depends on the wavelength, which highlights the difference in propagation speed between the two states. Furthermore, for both states, the intensity is maximum when phase matching occurs, which is mediated by LO phonons, as seen from the experimental integrated SH intensity as a function of the wavelength.

2. Experimental setup and sample growing

Details of the growing process of the NCs are described in our previous work [26]. Briefly, vapor transport deposition (VTD) technique was used to grow ZnO NCs on a 500 nm SiO_2 film thermally grown on Si (111). Au nanoclusters of ~5 nm diameter were sputtered onto the film to act as catalyzers. Control of the O_2 and Zn partial pressures at the substrate position within the VTD furnace determines the final morphology of the nano-objects. Figure 1 shows scanning electron microscope (SEM) images of the NCs, which are randomly oriented and have a planar body with single-sided teeth. NCs are homogeneously distributed over a macroscopic surface (25 mm^2) with a high density of about ~0.5-1 NCs/μm^2. Statistical analysis on many SEM images shows that the dimensions of the combs are: teeth length l = (580 ± 160) nm, teeth period a = (180 ± 20) nm, teeth diameter and body height d = (79 ± 6) nm and body width w = (190 ± 40) nm. Figure 1(b) shows hexagonal shaped teeth tips, supporting the fact that the growth direction of those nanowires is along the c axis of wurtzite ZnO, as has been reported in other similar works [27, 28].

#197588 - $15.00 USD Received 12 Sep 2013; revised 25 Nov 2013; accepted 5 Jan 2014; published 28 Feb 2014

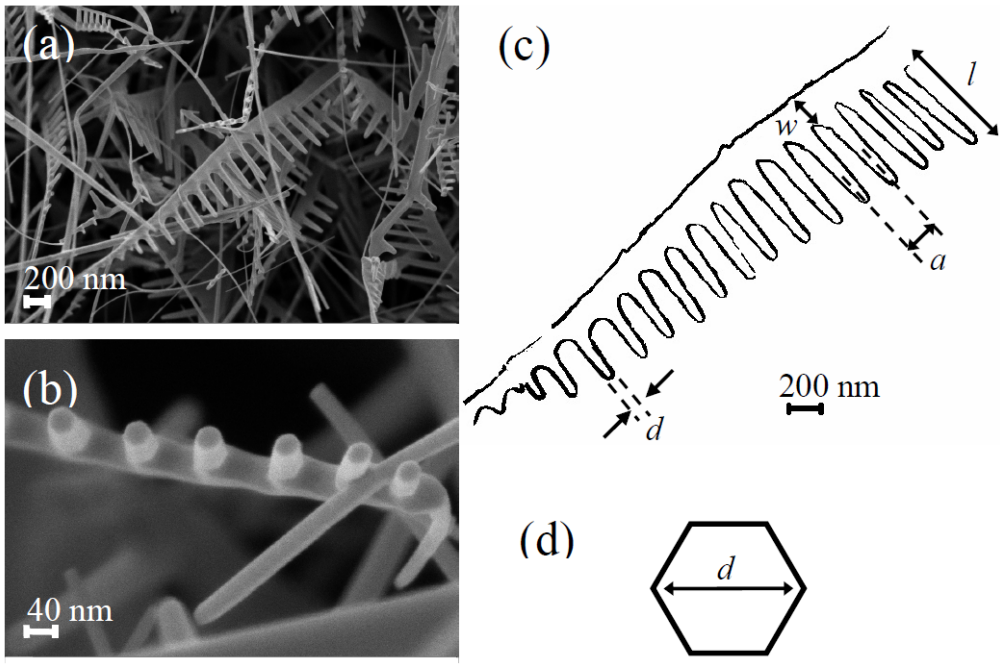

Fig. 1. (a), (b) SEM images and (c), (d) geometrical description of the ZnO nanocombs (NCs). SEM images show a high density of randomly oriented NCs. In a close view into the tip of the teeth, the hexagonal shape can be seen, indicating that teeth are aligned with the *c* crystalline axis of wurtzite ZnO. NCs characteristic dimensions (see text for the measured values) are shown in (c) and (d).

Room temperature optical spectra were obtained by using a linearly polarized Ti:Sapphire (Ti:Sa) pulsed laser as the excitation source, with 180 mW of average power and 70 fs pulse width with a repetition rate of 90 MHz. The wavelength has been tuned from 760 nm to 805 nm (1.54 eV to 1.63 eV). The laser beam was focused down onto a spot of ~1.2 μm^2 using a long-working distance microscope objective. The scattered light was collected in back-scattering geometry and sent to a double-grating Raman spectrometer (Jobin Yvon U1000) with liquid nitrogen cooled CCD detection. By comparison of the laser beam spot size and the size of the NCs we assume that only few teeth of a single NC fall within the laser spot, and consequently, our measurements are essentially taken on single NCs. Additional experimental findings corroborate this hypothesis. First, we have found the same type of emission spectrum on different regions of the sample, which is reasonable since basically at any part in the sample there is a NC. However, for a fixed spot in the sample, rotating the laser polarization could reduce the emission intensity from thousands of counts to a few tens (indicating strong polarization dependence, presented and discussed in the following section). When translating the sample across the laser spot a few micrometers, the rotation angle (for the polarization) required for this effect is completely different, as expected from the random orientation of the NCs. If we had been measuring an average emission from multiple NCs on different positions of the sample, these effects would have not have been observed, supporting our hypothesis of single NC detection.

3. Results and discussion

ZnO has wurtzite crystalline structure allowing the existence of three free exciton (FX) transitions called FX*A*, FX*B* and FX*C*, with measurable photoluminescence (PL) emission for the three of them at low temperature, together with the emission of bound-excitons, which disappears above a temperature of about 150 K [29]. The symmetry of the FX*A* and FX*B* excitons allows excitation with electric field polarized perpendicular to the *c* axis, while the

#197588 - $15.00 USD Received 12 Sep 2013; revised 25 Nov 2013; accepted 5 Jan 2014; published 28 Feb 2014

exciton FX*C* with a field polarized parallel to the *c*-axis [30, 31]. Room temperature emission shows a broad peak, from which it is difficult to assign the energy for each separated exciton. Accepted values for room temperature excitons energies range from 3.30 eV to 3.36 eV [2, 7, 19, 20, 26, 29, 30, 32].

SH generation near excitonic resonances in ZnO is a coherent optical process, for which two photon-like polaritons in the near infrared are combined to create one exciton-like polariton in the UV. If twice the energy of the pumping photon is above the ZnO band-gap, incoherent PL induced by two-photon absorption (TPPL) is the main light emission process, whereas below the band-gap SH generation dominates. ZnO is a birrefringent uniaxial material for which the dielectric tensor has two independent elements, $\varepsilon_{//}$ and $\varepsilon_{\perp}$, where the subscripts refer to parallel or perpendicular to the *c* (optical) axis. The generation and propagation of the SH field in this material is strongly dominated by the polarization of the incident (fundamental) field and the angle of incidence. For either input polarizations *s* or *p*, the nonlinear polarization of the material and the SH field are *p*-polarized [18], but their relative intensities are determined by the relation between the d_{333} and d_{311} elements of the second-order nonlinear optical tensor of ZnO. The expression for the SH intensity renders [18]:

$$I_{2\omega} \propto I_{\omega}^{2} \left(\frac{2\pi l}{\lambda} \right)^{2} e^{-2\delta_{2\omega}} \frac{\sin^{2}\psi + \sin\mathrm{h}^{2}\,\delta_{2\omega}}{\psi^{2} + \delta_{2\omega}^{2}} d_{eff}^{2} \qquad (1)$$

where $\delta_{2\omega}$ is the absorption coefficient times length at the SH, I_{ω} and $I_{2\omega}$ are the intensities of the fundamental and SH beam respectively, and d_{eff} is the effective second-order nonlinear coefficient, dependent on d_{333}, d_{311} and the incident and refracted angle. $\Psi = (2\pi l/\lambda)(n_{\omega} \cos \theta_{\omega} - n_{2\omega} \cos \theta_{2\omega})$ is the phase mismatch, for which the refractive indices (n_{ω} and $n_{2\omega}$) are both extraordinary for *p*-polarized fundamental beam, whereas for *s*-polarized the refractive index is ordinary for the fundamental and extraordinary for the SH. As in both cases the SH waves are extraordinary, the SH electric field has components in directions parallel and perpendicular to the *c* axis, and then mixed-mode polaritons are produced in the material [30, 31].

Optical emission spectra at room temperature taken with *p*-polarized incident beam from a single NC are shown in Fig. 2(a). By tuning the laser from 1.56 eV to 1.63 eV, all the excitation energies are below half of the ZnO band-gap: 3.37 eV (368 nm) at room temperature [33]. Figure 2(a) shows that each emission spectrum is centered at double the energy of the excitation, *i.e.* at the SH energy. The log-log plot of the SH intensity as a function of the incident intensity yields a slope of 1.94 ± 0.01 (not shown), which is consistent with the expected quadratic behavior. It is evident that the total emission is mainly due to the SH, since the width and position in energy of the spectra is on the order of the expected values for pure SH. Moreover, since defect-related green emission present in ZnO NCs for above-half band gap excitation [20] disappears in our measurements, the contribution of the multi-photonic incoherent emission can be considered negligible in the present case of below-half band gap excitation. Additionally, to rule out possible heating effects we made experiments varying the incident power (not shown), and we observed that the emission spectra preserves the shape (only the amplitude changes), even for the highest incident power available.

Looking at the spectra of Fig. 2(a), a highly structured profile can be observed that corresponds to FP cavity modes, related to the SH mode confinement in the NC teeth. Note that the SH signal cannot come from the confinement of the fundamental beam in the cavity. If so, the spacing between FP modes would be greater than the width of the signal spectrum, rendering these modes undetectable. Also, confined modes in the direction normal to *c* could be present but, again, their separation would be greater than the spectral region observed. In order to analyze the cavity performance, we made a nonlinear fit with a sum of Lorentzians for each spectrum of Fig. 2(a). Figure 2(b) shows the specific case of an incident energy of 1.58 eV (SH, 3.16 eV). Each one of the Lorentzians is the signature of one FP mode, for

#197588 - $15.00 USD Received 12 Sep 2013; revised 25 Nov 2013; accepted 5 Jan 2014; published 28 Feb 2014

which the full width at half maximum (FWHM), spectral distance (Free Spectral Range, FSR) and spectral position are related to the quality factor (Q) and the finesse (f) of the cavity. From Fig. 2(a) we obtain Q = 582 ± 60, which is a rather high value if we compare with previous reports in similar systems [16], and f = 1.6 ± 0.2. Finesse can be expressed as

$$f = \frac{\pi}{2\arcsin(|1-R|/\sqrt{4R})} \tag{2}$$

where R is the reflectivity at the end surfaces of the cavity. By using the implicit Eq. (2), the reflectivity can be retrieved as R = 0.23 ± 0.03, which is on the order of magnitude of the values reported in the literature [1] for lasing nanowires and, is perhaps the highest value reported so far. This would be consistent with the hypothesis that the ZnO refractive index for the SH light increased as well, which would produce a higher index contrast with the surroundings.

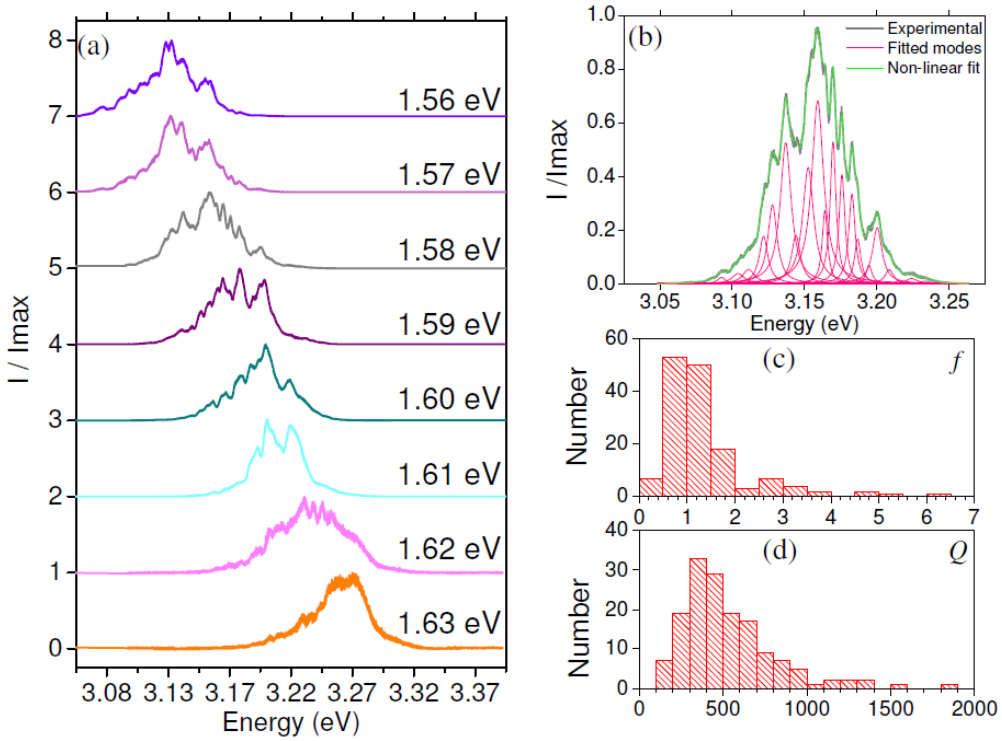

Fig. 2. (a) SH spectra of a single NC, for different incident photon energies. FP modes, which are the signature of SH confinement in the teeth cavities, are visible in each spectrum. (b) Detail of the spectrum at excitation energy of 1.58 eV. The nonlinear fit (green) is a sum of Lorentzians, corresponding to each FP mode (pink). (c) and (d) are the histograms of the finesse (f) and quality factor (Q), respectively, taken from the FP modes in all the measurements of (a).

A linear fitting of the energy maxima measured from Fig. 2(a) as a function of the mode number (with an arbitrary origin) leads to a mode spacing of 8.5 meV. The energy mode spacing (ΔE) in a FP cavity is given by $\Delta E = c_m \hbar \pi / l$, where c_m is the propagation velocity in the material and l is the cavity length. Considering a cavity length of (580 ± 160) nm, we get a propagation velocity of (2.4 ± 0.7) × 10^6 m/s. This velocity results to be 50 times smaller than the propagation velocity for non-interacting photons (1.2 × 10^8 m/s) that is obtained when using the background permittivity (6.2), and corresponds to the lowest values reported in the literature [5]. This behavior is expected when the mode volume is small enough to

#197588 - $15.00 USD Received 12 Sep 2013; revised 25 Nov 2013; accepted 5 Jan 2014; published 28 Feb 2014

enhance the interaction of photons and excitons due to the high confinement in the cavity, and consequently the material exhibits an increased Rabi splitting [5, 34]. In opposition, when pumping is high enough to produce very intense electric fields, the density of excitons could become higher than Mott density. In this case, excitonic binding energy is reduced by carrier screening, shrinking the Rabi splitting until no evidence of excitonic features can be seen in the dispersion relation [35]. In our experiment, both effects could act in competition (enhanced interaction and screening), which makes difficult to describe the proper polariton dispersion relation.

Following Eq. (1) and considering the refracted angles for the fundamental and SH beams similar, the highest SH emission will occur when the index of refraction of the fundamental beam equals the index of refraction of the SH. Since the propagation velocities of the fundamental photons and the SH photons are different, the nonlinear process is not perfectly phase-matched. However, as we will show next, efficient SH generation is possible due to a phonon-mediated interaction. The integrated intensity profile (ISH) for each measured spectrum, is shown as a function of the central SH energy in Fig. 3. The ISH shows its maxima for energies at FX-LO and FX-2LO, where the LO measured energy of (60 ± 10) meV agrees well with the reported values [36, 37]. In other words, the phonon contributes with the q_{ph} wavevector needed to fulfill the phase-matching condition. The measurement in Fig. 3 leads to an energy of 3.31 eV for the FX in this nanostructure.

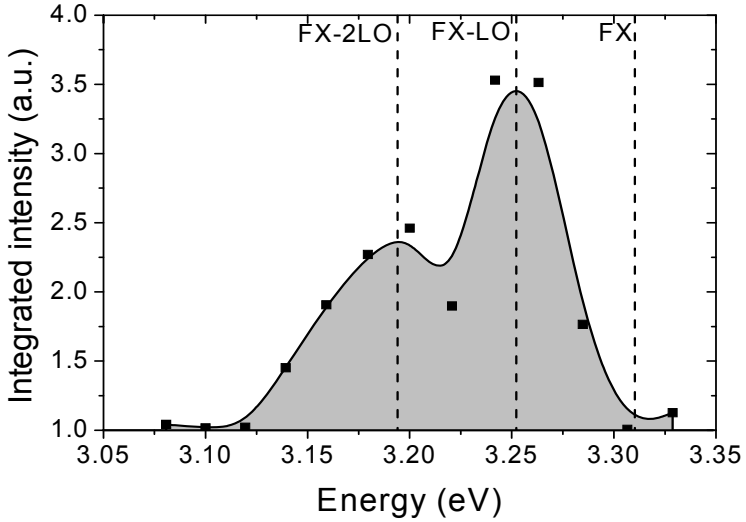

Fig. 3. Integrated SH intensity as a function of the SH energy. The energy maxima lie at the first and second phonon replicas.

Figure 4(a) sketches the geometry of our experiment, showing the cases of *p*-*p* (*p*-polarized fundamental and *p*-polarized SH) and *s*-*p* (*s*-polarized fundamental and *p*-polarized SH). SH generated with pump laser at 1.58 eV as a function of the polarization angle is shown in Fig. 4(b), for three different energies within the spectrum of the SH (3.18 eV, 3.16 eV and 3.15 eV). Results show that the SH intensity is strongly dependent on the polarization angle of the incident beam. For each wavelength the maximum is located near the *p*-*p* case (30°), whereas the polarization angle slightly shifts from one energy to the other due to the phase-matching condition achievement. In the *s*-*p* case, d_{eff} of Eq. (1) is proportional to the d_{311} coefficient, whereas in the *p*-*p* case both d_{333} and d_{311} take part [18]. However, as d_{333} is greater than d_{311} [18, 38], one can consider that in the high SH intensity state d_{333} dominates. We compute the contrast of polarization (*COP*) of the measurement as $COP = (I_{max}–I_{min})/(I_{max} + I_{min})$, where I_{max} and I_{min} correspond to the maximum and minimum intensities, respectively (Fig. 4(c)). The results show a high *COP* with values near 80% in all the range of energies we

#197588 - $15.00 USD Received 12 Sep 2013; revised 25 Nov 2013; accepted 5 Jan 2014; published 28 Feb 2014

measured. Figure 4(c) also shows secondary maxima at energies 3.145 eV, 3.152 eV, 3.160 eV (principal maximum), 3.169 eV, and 3.174 eV. Phase-matching condition given by Eq. (1) depends on the incoming wavelength for a given polarization. That means that ψ is slightly different for different wavelengths. When the *COP* is computed, these differences result in a modulation of the contrast, as shown in Fig. 4(c).

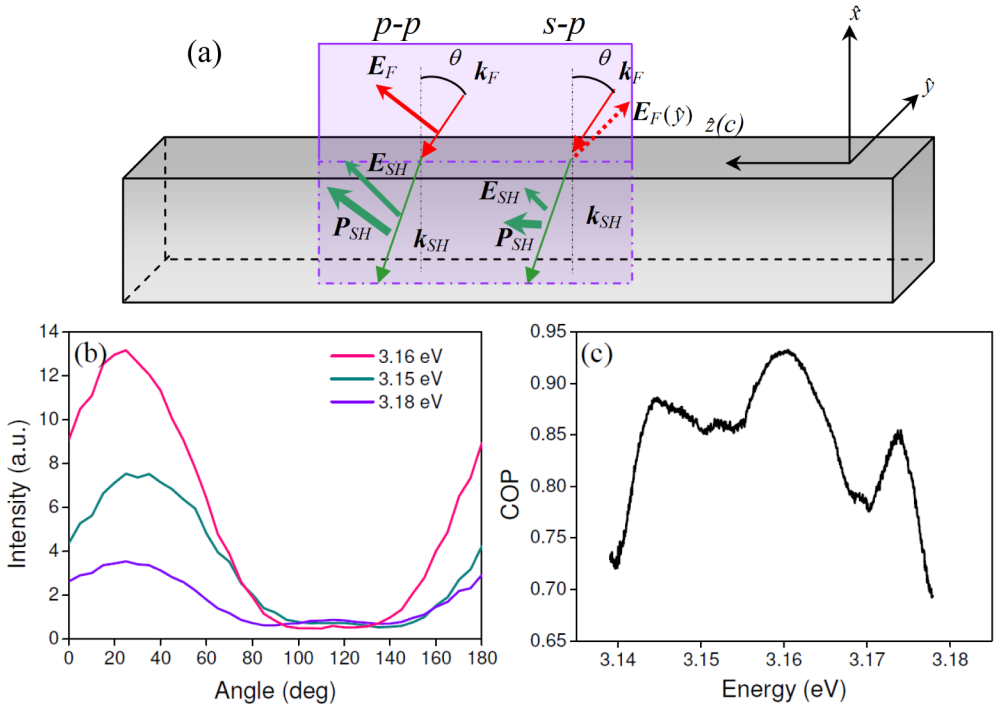

Fig. 4. (a) Sketch of the geometry of the experiment for *p-p* polarization and *s-p* polarization. $k_{F(SH)}$, $E_{F(SH)}$ are the wave vector and electric field of the fundamental *(SH)*, θ is the angle of incidence and P_{SH} is the non-linear polarization of the material. The *c* axis coincides with the *z* axis. (b) Intensity for 1.58 eV excitation energy as a function of the polarization angle of the incident beam, for three energies within the SH spectrum. (c) Contrast of polarization as a function of the SH energy.

4. Conclusions

In this work, we efficiently generated optical SH from single ZnO nanocombs with wide tunability from 3.0 eV to 3.3 eV. We also demonstrate that the SH couples to the nanocavity modes along the teeth of the ZnO nanocomb, showing typical FP resonances with high quality factors. Propagation velocity of the confined polaritons in the cavity is (2.4 ± 0.7) × 10^6 m/s, which is as far as we know the lowest reported velocity of the slowed down exciton-polariton in ZnO nano-microcavities. Looking at the SH integrated profile as a function of the incoming energy, we conclude that the phase matching condition is achieved mediated by LO phonons. By crossing input polarization, we can change the emission from high- to low-intensity states with high contrast, which can be viewed as a light switching mechanism in the nanoscale.

Acknowledgments

This work was supported by grants from Universidad de Buenos Aires (20020100100719 and 20020110300027) and Universidad Nacional de Tucumán (CIUNT 26/E419 and 26/E439) and grants from ANPCyT (Prestamo BID PICT Nº 2010-00825 and Nº 2010-00400). MGC,

GG, DC and AVB are members of CONICET. The authors gratefully acknowledge R. Merlin for fruitful discussions.

#197588 - $15.00 USD Received 12 Sep 2013; revised 25 Nov 2013; accepted 5 Jan 2014; published 28 Feb 2014